Mathematical Biosciences and Engineering

https://www.aimspress.com/journal/mbe

MBE, 23(7): 1886–1907.
DOI: 10.3934/mbe.2026069
Received: 22 December 2025
Revised: 03 April 2026
Accepted: 15 May 2026
Published: 30 June 2026

Research article

Stability properties of quadrature-based approximations for integral equations with delay terms

Eleonora Messina*and Claudia Panico

Department of Mathematics and Applications, University of Naples Federico II, via Cintia, I-80126 Naples, Italy.

* **Correspondence:** Email: eleonora.messina@unina.it.

Abstract: We study a class of linear integral equations involving both a discrete delay and a bounded distributed delay. Such equations, as well as their non-linear extensions, arise in the mathematical modelling of biological systems and in control theory. The equations are discretised using quadrature-based methods, and the resulting discrete schemes are analysed with respect to their stability properties. Sufficient conditions are derived under which the discrete formulation preserves the stability characteristics of the underlying continuous problem.

Keywords: Volterra integral equations; numerical stability; distributed delay; quadrature methods; stability regions; integral delay systems

1. Introduction

Volterra integral equations with delay provide a natural framework for modelling processes in which past states influence the present through memory or hereditary mechanisms. Delays of both discrete and distributed type arise in numerous scientific and engineering applications, and the resulting integral models capture temporal interactions that cannot be represented by instantaneous formulations. For comprehensive discussions on Volterra integral equations, we refer the reader to the monographs by Brunner [1], Gripenberg et al. [2], and Bellman and Cooke [3, Ch. 7–8].

In this paper, we consider the following linear integral equation of Volterra type:

$$y(t) = a\, y(t-\bar{\tau}) + b \int_0^{\bar{\tau}} k(\tau)\, y(t-\tau)\, d\tau, \qquad t > 0, \tag{1.1}$$

where $a,\ b \in \mathbb{R}$ and the kernel function $k : [0, \bar{\tau}] \to \mathbb{R}$ is continuous and positive. The parameter $\bar{\tau} > 0$ denotes the constant delay, and the initial condition is prescribed by a continuous function $\varphi(t)$ for $t \in [-\bar{\tau}, 0]$.

Equations with both pointwise and distributed delays arise naturally in epidemic renewal models with finite infectivity support; see, e.g., [4,5]. After reformulation with constant delay and linearisation around an equilibrium, one is led to linear systems with the same structural features. Equation (1.1) is used here as a scalar prototype of that class in order to isolate the combined effect of the two delay mechanisms and study whether a numerical discretisation preserves stability.

Related delayed integral structures also arise in other applications, including population and epidemic dynamics (Meehan *et al.* [5], Hritonenko et al. [4], Hethcote et al. [6], Beretta and Breda [7]), propagation phenomena in excitable media (Courtemanche et al. [8]), and control theory for networks of hyperbolic partial differential equations (Balogoun et al. [9]).

On the theoretical side, notable contributions to the analysis of systems of the form (1.1) include the spectral characterisations of stability by Auriol [10] and Balogoun et al. [9], as well as the Lyapunov–Krasovskii approaches developed by Melchor-Aguilar [11, 12], which yield sufficient conditions for exponential stability. Other studies consider a neutral-type equation obtained from (1.1) through a differential transformation, when the kernel k is differentiable; the spectrum of this transformed equation contains that of the original integral equation (Ochoa-Ortega and Gómez [13]).

The numerical solution of Volterra integral equations has been extensively investigated over the past decades. A general treatment of the subject can be found in the monograph by Brunner and van der Houwen [14]. Recent contributions include, among others, the works of Buonomo et al. [15], Messina et al. [16], Ripoll and Font [17], and Wendler et al. [18], which develop numerical methods specifically designed for integral models arising in ecology and infectious disease dynamics.

For Volterra equations with delay, recent advances have been reported by Abdi et al. [19], Hosseinian et al. [20], Conte et al. [21], and Darania and Sotoudehmaram [22]. A general overview of collocation methods is provided in Brunner's monograph [23]. Quadrature-based approaches have been proposed and analysed by Baker and Ford [24], Baker and Derakhshan [25], Luzyanina et al. [26], and Messina et al. [27].

Historically, the numerical analysis of Volterra equations also includes the classical Runge–Kutta framework developed by Lubich [28], which remains a fundamental reference for discretisations of Volterra and Abel equations. Stability issues for linear multistep discretisations of Volterra convolution equations were also studied by Lubich [29]. These contributions provide important background for the present study.
Moreover, the spectral viewpoint adopted below has clear analogies with the stability analysis of delay differential equations, where characteristic roots and boundary-locus techniques also play a central role; see, for instance, Shampine and Thompson [30] for a general overview and Breda, Maset, and Vermiglio [31] for a numerical treatment of stability based on spectral approximations.

More recently, AI-based and hybrid symbolic-learning approaches have been explored in related contexts, including reinforcement-learning strategies for non-linear integral equations [32], Physics-Informed Neural Network (PINN)-based and distributed symbolic-discovery techniques for fractional Volterra population models [33], and neural network architectures for fractional differential and integro-differential problems [34].

Despite the importance of integral equations characterized by both pointwise and distributed delays in a wide range of applications, their numerical approximation and stability properties have not yet been systematically investigated, to the best of our knowledge.

The objective of the present study is to address this topic. We propose a discretisation based on

Gregory-type quadrature formulas and carry out a stability analysis of the resulting numerical solution to (1.1). We adopt a Laplace transform-based approach, which provides a unified framework for analysing both the continuous system and its discrete counterpart. This alignment with existing spectral techniques enables a consistent comparison between analytical and numerical stability domains.

The paper is organised as follows. Section 2 introduces the theoretical framework and presents the stability analysis of the continuous system. Section 3 develops the numerical scheme and examines its stability properties. Section 4 discusses sufficient stability conditions and spectral-set comparisons for general kernel-functions. Concluding remarks are given in Section 5.

2. Theoretical framework

We consider Volterra delay integral equations of the type (1.1), and we refer to Anselone and Greenspan [35] for the existence and uniqueness theory of solutions in $C[0,+\infty)$. In the following, we provide results about the smoothness of this solution and its asymptotic behaviour.

2.1. Existence and regularity of solutions

Theorem 2.1. *Assume that the given functions k, φ possess continuous derivatives of at least order $m \geq 1$ on their respective domains. Then, for any positive integer M, there exists a unique solution y of (1.1) on $(0, M\bar{\tau}]$, with $y \in C^m(\bar{\tau}_j, \bar{\tau}_{j+1}]$ for $j = 0, \ldots, M-1$, where $\bar{\tau}_j = j\bar{\tau}$. Moreover, y is bounded on $[0, M\bar{\tau}]$.*

If the initial function φ satisfies

$$\varphi(0) = a\,\varphi(-\bar{\tau}) + b \int_0^{\bar{\tau}} k(\tau)\,\varphi(-\tau)\,d\tau, \tag{2.1}$$

then the solution is continuous at all delay points $t = \bar{\tau}_j$.

Proof. Locally in the interval $(0, \bar{\tau}]$, equation (1.1) may be written as a Volterra equation:

$$y_1(t) = F_0(t) + b \int_0^{t} k(t-\tau)\,y_1(\tau)\,d\tau, \tag{2.2}$$

where

$$F_0(t) = a\,\varphi(t-\bar{\tau}) + b \int_{t-\bar{\tau}}^{0} k(t-\tau)\,\varphi(\tau)\,d\tau.$$

From the regularity assumptions on the given functions, it follows that $F_0(t) \in C^m(0, \bar{\tau}]$, and hence by applying the classical Volterra theory (see, for example, Brunner [1, Sec.1.2.1]), $y_1(t) \in C^m(0, \bar{\tau}]$ as well. Furthermore,

$$y(0^+) = \lim_{t \to 0^+} y_1(t) = a\,\varphi(-\bar{\tau}) + b \int_0^{\bar{\tau}} k(\tau)\,\varphi(-\tau)\,d\tau,$$

which, for general continuous data functions k and φ, does not coincide with $\varphi(0)$. Continuity at $t = 0$ (that is, $y(0^+) = \varphi(0)$) holds if (2.1) is satisfied.

By proceeding recursively on the intervals $[\bar{\tau}_j, \bar{\tau}_{j+1}]$, $j = 0, \ldots, M-1$, using the method of steps, and rewriting (1.1) at each stage as a classical Volterra equation, one readily obtains that

$$y \in C^m\left(\bar{\tau}_j, \bar{\tau}_{j+1}\right].$$

and

$$y(\bar{\tau}_{j+1}^-) - y(\bar{\tau}_{j+1}^+) = a\left(y(\bar{\tau}_j^-) - y(\bar{\tau}_j^+)\right) < +\infty, \quad j = 0, 1, \ldots, M-1.$$

Moreover, if condition (2.1) is satisfied, then $y(\bar{\tau}_{j+1}^-) - y(\bar{\tau}_{j+1}^+) = 0,\ j = 0, 1, \ldots, M-1.$ □

Remark 2.1. *The smoothing effect is only local. More precisely, on each interval* $(j\bar{\tau}, (j+1)\bar{\tau}]$*, equation* (1.1) *behaves like a Volterra integral equation with a smooth inhomogeneous term, so the solution is smooth inside that interval. At the delay points* $t = j\bar{\tau}$*, however, the term* $a\,y(t-\bar{\tau})$ *connects one step to the next without imposing any extra matching conditions on the derivatives. Therefore, condition* (2.1) *guarantees continuity of the solution at the delay points, but the derivatives may still be discontinuous there.*

2.2. Asymptotic properties

We consider the asymptotic stability of the linear delay integral equation described by (1.1). Taking the Laplace transform of (1.1) leads to

$$\hat{Y}(\omega) = (a\,e^{-\omega\bar{\tau}} + b\hat{k}(\omega))\hat{Y}(\omega) + a\,e^{-\omega\bar{\tau}}\hat{\Phi}(\omega) + b\,G(\omega), \tag{2.3}$$

where

$$\begin{aligned} \hat{Y}(\omega) &= \int_0^\infty e^{-\omega\tau} y(\tau)\,d\tau, \qquad \hat{\Phi}(\omega) = \int_{-\bar{\tau}}^0 e^{-\omega\tau}\varphi(\tau)\,d\tau, \\ G(\omega) &= \int_0^{\bar{\tau}} e^{-\omega\tau} k(\tau) \int_{-\tau}^0 e^{-\omega s}\varphi(s)\,ds\,d\tau, \end{aligned}$$

and $\hat{k}$ is the Laplace transform of the function agreeing with $k(t)$ for $t \in [0, \bar{\tau}]$ and vanishing elsewhere,

$$\hat{k}(\omega) = \int_0^{\bar{\tau}} e^{-\omega\tau} k(\tau)\,d\tau.$$

In order to study the asymptotic stability of the zero solution, we use the final value theorem of the Laplace transform [36] and introduce the stability function

$$D(a, b; \omega) = 1 - ae^{-\omega\bar{\tau}} - b\hat{k}(\omega). \tag{2.4}$$

Equivalently, one may seek solutions of exponential type $y(t) = e^{\omega t}$ in (1.1), which again yields the characteristic equation $D(a, b; \omega) = 0$. Thus, the corresponding characteristic roots ω determine the relevant spectral bound and, therefore, the asymptotic stability of the zero solution; see, e.g., Bellman and Cooke [3] and Gripenberg et al. [2].

Since the characteristic equation is transcendental, it may have infinitely many characteristic roots. However, for the present delay-integral equation, only finitely many roots can lie in any right half-plane $Re(\omega) > \eta$; see, e.g., [26, 37]. Therefore, asymptotic stability is determined by the location of the rightmost characteristic roots.

Theorem 2.2. *The zero solution of (1.1) is asymptotically stable if and only if the characteristic equation*

$$D(a, b; \omega) = 0, \tag{2.5}$$

with D defined in (2.4)*, has all its roots in the left half-plane* $Re(\omega) < 0$.

Thus, a given pair (a, b) yields a stable equation (1.1) if and only if the characteristic equation (2.5) has no roots in the closed right half-plane.

Remark 2.2. *The existence and regularity result of Theorem 2.1 holds for arbitrary $a \in \mathbb{R}$. In the analysis of the continuous and discrete stability regions developed below, the restriction $|a| < 1$ is adopted only as a reference strip. This choice allows for a direct comparison between the continuous boundary and its quadrature-based discrete counterpart in the parameter regime most commonly considered in the literature (see, e.g., [9] and the references therein). This construction is not confined, in principle, to this strip, but a systematic analysis outside it is beyond the scope of the present work.*

According to Remark 2.2, the continuous and discrete stability regions are now considered in the strip $(-1, 1) \times \mathbb{R}$. Let $S \subset \mathbb{R}^2$ be the set of such (a, b) where stability holds:

$$S := \{(a, b) \in (-1, 1) \times \mathbb{R} : D(a, b; \omega) \neq 0 \text{ for all } \omega \text{ with } Re(\omega) \geq 0\}. \tag{2.6}$$

In order to draw the boundary ∂S of the *stability region* S, we use the method of D-partitions as described by Baker and Ford [24].
The (a, b)-plane is partitioned into different regions by means of the curve branches defined by

$$a = a(\beta), \quad b = b(\beta), \quad \beta \in \mathbb{R}, \tag{2.7}$$

characterized by the corresponding characteristic equation (2.5) having at least one zero on the imaginary axis:

$$D(a(\beta), b(\beta); i\beta) = 0. \tag{2.8}$$

The points in the interior of each region correspond to a characteristic equation with the same number of roots having a positive real part. The set S (which may be disconnected) is the union of all the regions where no such roots exist.

Referring to the stability function (2.4), equation (2.8) turns into the following system:

$$\begin{cases} 1 - a\cos\beta\bar{\tau} - b\int_0^{\bar{\tau}} k(\tau)\cos\beta\tau\, d\tau = 0, \\ a\sin\beta\bar{\tau} + b\int_0^{\bar{\tau}} k(\tau)\sin\beta\tau\, d\tau = 0. \end{cases} \tag{2.9}$$

Therefore, the points $(a(\beta), b(\beta))$ that satisfy the system (2.9), along with the solutions arising in case the coefficient matrix is singular (which correspond to a straight line), contribute to the boundary of the partition.

When $\beta = 0$, the system admits solutions represented by the straight line:

$$a + b\int_0^{\bar{\tau}} k(\tau)\, d\tau = 1. \tag{2.10}$$

Equation (2.10) defines the boundary of a first partition in the (a, b)-plane. Furthermore, by a straightforward application of Lemma 2 proved by Balogoun et al. [9], equation (1.1) cannot be stable if $a + b\int_0^{\bar{\tau}} k(\tau)\, d\tau \geq 1$. Hence, the stability region S is located below the line defined by (2.10).

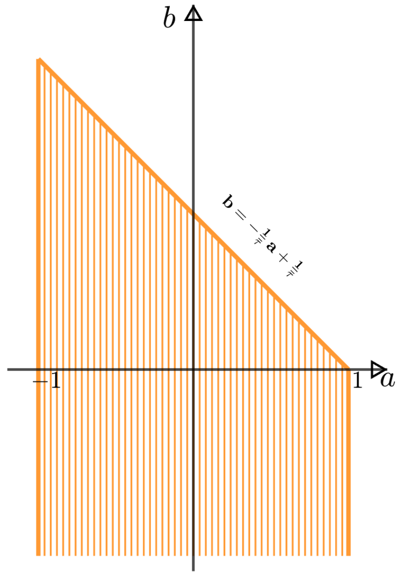

Figure 1. Schematic representation of the strip $(-1, 1) \times \mathbb{R}$ and of the straight line $a + b\bar{\tau} = 1$, which forms the upper boundary of the continuous stability region for the basic test equation $k(\tau) = 1$.

For $\beta \neq 0$, an analysis on system (2.9) to determine ∂S analytically is, in general, difficult for arbitrary continuous kernel k. Thus, we turn our attention to equation (1.1) with $k(t) = 1$, the so-called *basic test equation*. In this case, from (2.10), we deduce that $\beta = 0$ gives the line

$$a + b\bar{\tau} = 1. \tag{2.11}$$

When $\beta \neq 0$, simple manipulations lead to the following system:

$$\begin{cases} \beta - a\beta\cos\beta\bar{\tau} - b\sin\beta\bar{\tau} = 0, \\ a\beta\sin\beta\bar{\tau} - b(\cos\beta\bar{\tau} - 1) = 0, \end{cases} \tag{2.12}$$

whose coefficient matrix is singular for $\beta = \frac{2k\pi}{\bar{\tau}}$, $k \in \mathbb{Z} - \{0\}$, corresponding to the line $a = 1$. The singular case therefore identifies the straight line $a = 1$, showing that the D-partition naturally extends beyond the reference strip adopted here. All the other values of $\beta \neq \frac{2k\pi}{\bar{\tau}}$, $k \in \mathbb{Z}$ give points $(a, b) = \left(-1, \frac{\beta\sin(\beta\bar{\tau})}{1-\cos(\beta\bar{\tau})}\right)$. These points belong to the branch $a = -1$, that is, to the boundary of the strip $-1 < a < 1$ considered here.

Figure 1 provides a schematic geometric representation of the strip $(-1, 1) \times \mathbb{R}$ and of the straight line $a + b\bar{\tau} = 1$, which forms the upper boundary of the continuous stability region in the basic test equation.

3. The discretised equation

Let $\Pi_n = \{t_n = nh, n = 0, 1, \ldots\}$, where $h > 0$ is the stepsize of the discretisation, which we assume to be constrained by $\bar{r}h = \bar{\tau}$, $\bar{r}$ positive and integer. A quadrature-based method for the numerical solution to (1.1) reads

$$y_n = ay_{n-\bar{r}} + bh \sum_{j=0}^{\bar{r}} w_j k(t_j) y_{n-j}, \tag{3.1}$$

where $y_n \approx y(t_n)$, $n = 0, 1, \ldots$ and $y_j = \varphi(t_j)$, $j = -\bar{r}, \ldots, -1$, where φ is the given initial function. The coefficients w_j, $j = 0, \ldots, \bar{r}$ are the weights of a quadrature formula. We choose the class of Gregory quadrature formulas, and we refer to [14] for details about the construction and analysis of these methods. We recall that the base case of the Gregory formulas corresponds to the *trapezoidal rule*, which is of order $p = 2$. Higher-order formulas ($p > 2$) are derived by modifying the trapezoidal weights through q-corrections applied near the endpoints of the integration interval ($q = 0$ in the trapezoidal case). As a consequence, only the first and last $q + 1$ weights differ from unity, and these weights are symmetric, i.e.,

$$w_j = w_{\bar{r}-j}, \quad j = 0, \ldots, q,$$

while $w_j = 1, \quad j = q + 1, \ldots, \bar{r} - q - 1$.

This structural property makes Gregory quadrature particularly suitable for the numerical solution of Volterra integral equations, as well as for general integration problems without restrictions on the number of nodes. It can be shown that, for sufficiently smooth integrands, the q-th Gregory formula achieves order $p = q + 2$ and is exact for all polynomials of degree up to $q + 1$.

3.1. Convergence

By applying the classical theory on convergence (based on discrete Gronwall-type inequalities), the method of steps, and the fact that the discontinuity points for the derivatives of y, $\bar{\tau}_j = j\bar{\tau}$, $j = 0, 1, \ldots$, are included in the mesh Π_n, the following result holds.

Theorem 3.1. *Let M be a fixed positive integer. Assume that, for equation* (1.1), $k \in C^p[0, \bar{\tau}]$ *and* $\varphi \in C^p[-\bar{\tau}, 0]$, *where p is the order of the underlying quadrature formula. Then, for all sufficiently small stepsizes h satisfying the constrained mesh condition $\bar{r}h = \bar{\tau}$, the numerical solution $\{y_n\}$ produced by (3.1) satisfies*

$$\max_{n=0,\ldots,M\bar{r}} |y(t_n) - y_n| \leq Ch^p$$

for some constant $C > 0$ not depending on h.

Figure 2 illustrates the convergence result of Theorem 3.1 by means of a forced test problem associated with (1.1). The forcing term $f(t)$ is chosen so that the exact solution is $y(t) = t$. Accordingly, the initial function is taken as $\varphi(t) = t$ on $[-\bar{\tau}, 0]$, which satisfies the compatibility condition (2.1). The experiment is performed with $\bar{\tau} = 1$, $a = 0.1$, $b = -0.1$, and $k(\tau) = 1/(1 + \tau^2)$ over the interval $[0, 5]$. Figure 2 reports the endpoint error versus h for methods (3.1) of order $p = 2, \ldots, 6$, together with the corresponding theoretical slopes.

3.2. Stability for a general kernel

In analogy with Section 2.2, we study the asymptotic stability of the discrete scheme (3.1) through its characteristic equation. To this end, we look for solutions of the form $y_n = z^n$, with $z \in \mathbb{C}$. Substitu-

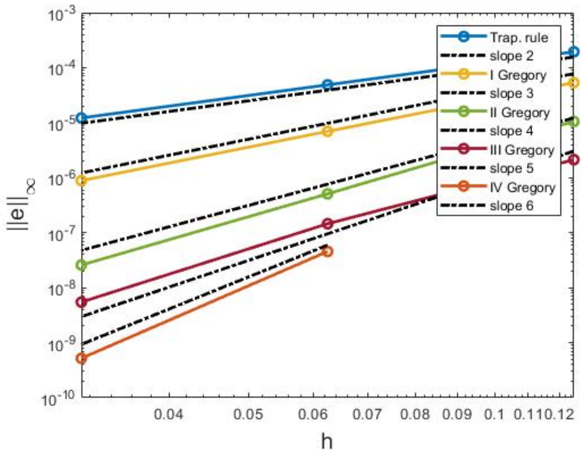

Figure 2. Endpoint error versus h for the forced counterpart of (1.1), with exact solution $y(t) = t$ and initial function $\varphi(t) = t$ on $[-\bar{\tau}, 0]$, $\bar{\tau} = 1$, $a = .1$, $b = -.1$, and $k(\tau) = 1/(1+\tau^2)$. The dash-dotted lines indicate the corresponding theoretical convergence orders.

tion into (3.1) gives

$$\widetilde{D}_h(a, b; z) := z^{\bar{r}} - a - bh \sum_{j=0}^{\bar{r}} w_j k(t_j) z^{\bar{r}-j} = 0. \tag{3.2}$$

Equivalently, for $z \neq 0$, we introduce the associated stability function

$$D_h(a, b; z) := z^{-\bar{r}} \widetilde{D}_h(a, b; z) = 1 - a z^{-\bar{r}} - bh \sum_{j=0}^{\bar{r}} w_j k(t_j) z^{-j}, \tag{3.3}$$

which is in agreement with the classical z-transform framework for linear difference equations; see, for instance, [38]. The discrete counterpart of Theorem 2.2 can then be stated as follows.

Theorem 3.2. *The zero solution of (3.1) is asymptotically stable if and only if all the roots of*

$$\widetilde{D}_h(a, b; z) = 0$$

lie in the open unit disk $|z| < 1$. *Equivalently, this holds if and only if*

$$D_h(a, b; z) \neq 0 \qquad \textit{for all } |z| \geq 1.$$

As in Section 2.2, for each fixed admissible $h > 0$, we restrict the subsequent boundary-locus analysis to the strip $(-1, 1) \times \mathbb{R}$. Accordingly, we define the discrete stability region

$$S_h = \{(a, b) \in (-1, 1) \times \mathbb{R} : \; D_h(a, b; z) \neq 0 \text{ for all } |z| \geq 1\}.$$

We apply the boundary-locus technique described by Baker and Ford [24] in direct analogy with the continuous analysis of Section 2.2. To parametrize the unit circle, let

$$z = e^{i\theta h}, \qquad \theta \in \left[0, \frac{2\pi}{h}\right].$$

Then the boundary locus in the (a, b)-plane is determined by the condition

$$D_h(a(\theta), b(\theta); e^{i\theta h}) = 0.$$

For the stability function (3.3), this is equivalent to the system

$$\begin{cases} a\cos\theta\bar{\tau} + bh\displaystyle\sum_{j=0}^{\bar{r}} w_j k(t_j)\cos\theta jh = 1, \\ a\sin\theta\bar{\tau} + bh\displaystyle\sum_{j=0}^{\bar{r}} w_j k(t_j)\sin\theta jh = 0, \end{cases} \tag{3.4}$$

which yields either regular boundary points or, in the singular case, straight lines contributing to the boundary of S_h.

At the endpoint values $\theta = 0$ and $\theta = 2\pi/h$, which both correspond to $z = 1$, system (3.4) is singular, and the solutions lie on the straight line

$$a + bh\sum_{j=0}^{\bar{r}} w_j k(t_j) = 1. \tag{3.5}$$

Furthermore,

$$D_h(a, b; 1) = 1 - a - bh\sum_{j=0}^{\bar{r}} w_j k(t_j),$$

so the straight line (3.5) corresponds to the passage of a characteristic root through $z = 1$ and therefore contributes to the boundary of the stability region S_h.

To compare the continuous and discrete boundary loci, we rewrite systems (2.9) and (3.4) in matrix form. Writing $z = e^{i\beta h}$, for each fixed $\beta \in \mathbb{R}$, we have

$$M(\beta)x(\beta) = \begin{pmatrix} 1 \\ 0 \end{pmatrix}, \qquad M_h(\beta)x_h(\beta) = \begin{pmatrix} 1 \\ 0 \end{pmatrix},$$

where

$$M(\beta) = \begin{pmatrix} \cos(\beta\bar{\tau}) & \displaystyle\int_0^{\bar{\tau}} k(s)\cos(\beta s)\,ds \\ \sin(\beta\bar{\tau}) & \displaystyle\int_0^{\bar{\tau}} k(s)\sin(\beta s)\,ds \end{pmatrix}, \qquad x(\beta) = \begin{pmatrix} a(\beta) \\ b(\beta) \end{pmatrix},$$

and

$$M_h(\beta) = \begin{pmatrix} \cos(\beta\bar{\tau}) & h\displaystyle\sum_{j=0}^{\bar{r}} w_j k(t_j)\cos(\beta jh) \\ \sin(\beta\bar{\tau}) & h\displaystyle\sum_{j=0}^{\bar{r}} w_j k(t_j)\sin(\beta jh) \end{pmatrix}, \qquad x_h(\beta) = \begin{pmatrix} a_h(\beta) \\ b_h(\beta) \end{pmatrix}.$$

Hence, away from singular configurations, the difference between the continuous and discrete boundary points is determined by the quadrature errors in $\int_0^{\bar{\tau}} k(\tau)\cos(\beta\tau)\,d\tau$ and $\int_0^{\bar{\tau}} k(\tau)\sin(\beta\tau)\,d\tau$. Indeed, writing $M_h(\beta) = M(\beta) + E_h(\beta)$, we obtain, whenever $M(\beta)$ is nonsingular,

$$x_h(\beta) - x(\beta) = -\left(M(\beta) + E_h(\beta)\right)^{-1} E_h(\beta)x(\beta).$$

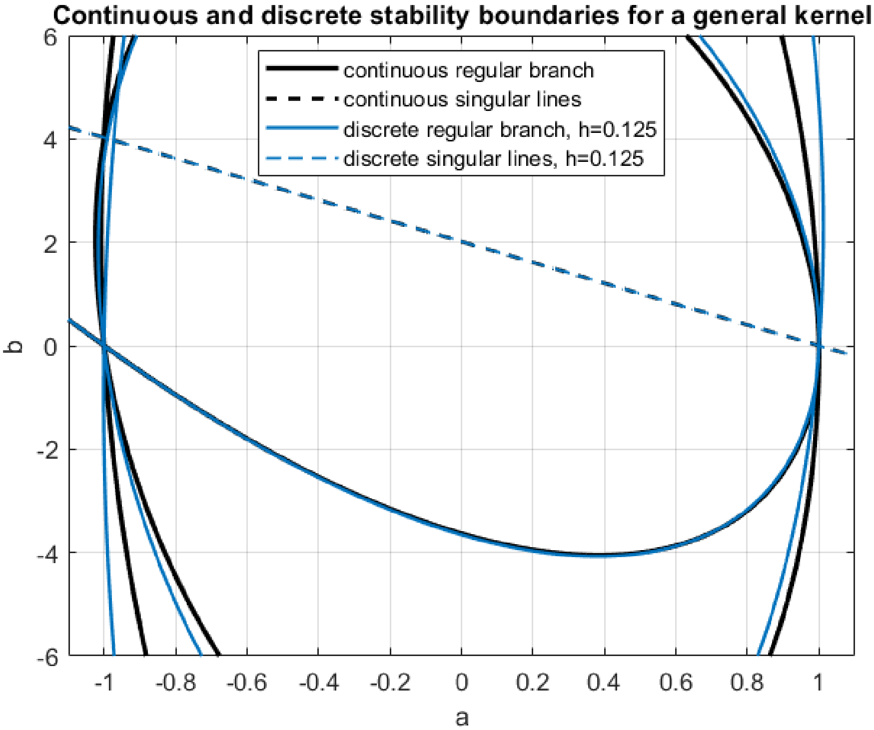

Figure 3. Continuous and discrete stability boundaries for the non-constant kernel $k(\tau) = \tau e^{-0.01\tau}$, with $\bar{\tau} = 1$. The discrete boundaries are computed by the Gregory method of order $p = 3$ and with stepsize $h = 0.125$.

If the kernel k is sufficiently smooth, then the entries of $E_h(\beta)$ are of the same order as the quadrature errors in the two integrals above. Hence, $E_h(\beta) = O(h^p)$ as $h \to 0$, where p is the order of the underlying quadrature formula. Therefore, for each fixed β such that $M(\beta)$ is nonsingular and uniformly well conditioned, standard perturbation arguments imply that

$$x_h(\beta) - x(\beta) = O(h^p)$$

so that the discrete boundary point $(a_h(\beta), b_h(\beta))$ approximates the continuous one $(a(\beta), b(\beta))$ with the same order.

To illustrate this behaviour, we consider the kernel $k(\tau) = \tau e^{-0.01\tau}$ with $\bar{\tau} = 1$. In Figure 3, we compare the continuous and discrete stability boundaries. The continuous boundary is obtained from (2.9), while the discrete one is obtained from (3.4) with stepsize $h = 0.125$. Both the regular branch and the singular lines are accurately reproduced by the discrete approximation, showing that the stability boundary for a general kernel can be effectively reconstructed from the corresponding quadrature approximations. In order to visualize the local effect of the quadrature error on the boundary reconstruction, we also fix a frequency value $\beta = 5$, which lies away from the singular configurations, and compare the corresponding errors in $a_h(\beta)$ and $b_h(\beta)$. The decay of the errors shown in Figure 4 is consistent with the order of the underlying quadrature formula and in agreement with the perturbation estimate above.

The general-kernel setting clarifies the role of the quadrature approximation in the reconstruction of

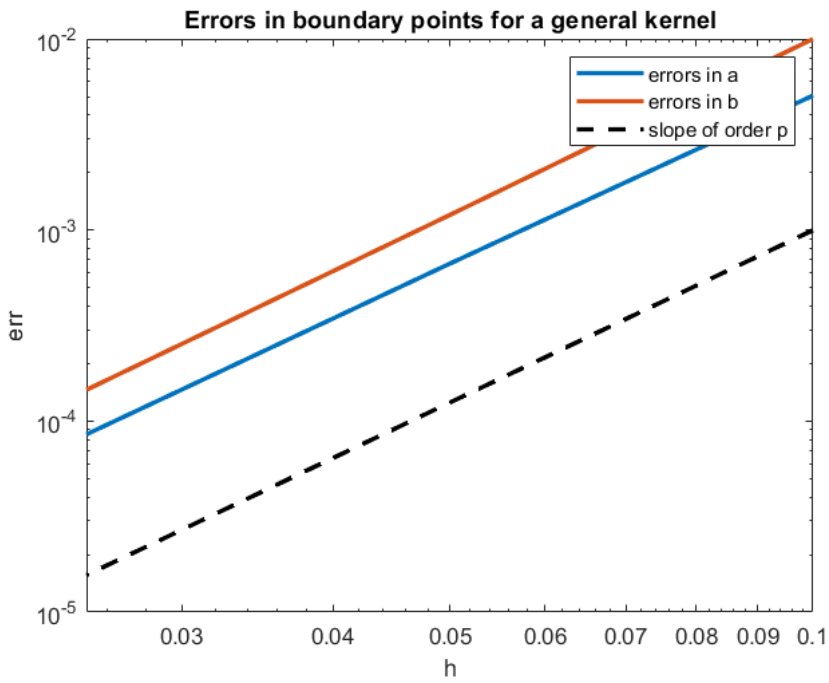

Figure 4. Errors in the reconstructed boundary point $(a_h(\beta), b_h(\beta))$ for the kernel $k(\tau) = \tau e^{-0.01\tau}$, with $\bar{\tau} = 1$, Gregory method of order $p = 3$, and fixed frequency $\beta = 5$.

the stability boundary. In the particular case $k(\tau) = 1$, this analysis can be further specialized, leading to more explicit formulas and sharper information on the geometry of the discrete stability region.

3.3. *The basic test equation*

We now specialize the previous analysis to the basic test equation, that is, to (3.1) with constant kernel $k(\tau) = 1$. In this case, the singular line (3.5) becomes $a + b\bar{\tau} = 1$, which coincides with the upper boundary (2.11) of the continuous stability region. Moreover, exploiting the symmetry of the quadrature weights w_j, $j = 0, \ldots, \bar{r}$, the stability function D_h can be rewritten as

$$D_h(a(\theta), b(\theta); e^{i\theta h}) = 1 - ae^{-i\theta\bar{\tau}} - be^{-i\theta\frac{\bar{\tau}}{2}} Q(\theta; h),$$

with

$$Q(\theta; h) = \begin{cases} 2h \displaystyle\sum_{j=0}^{(\bar{r}-1)/2} w_j \cos\left(\frac{\theta}{2} h(\bar{r} - 2j)\right), & \bar{r} \text{ odd}, \\ h\left(2 \displaystyle\sum_{j=0}^{\bar{r}/2-1} w_j \cos\left(\frac{\theta}{2} h(\bar{r} - 2j)\right) + 1\right), & \bar{r} \text{ even}. \end{cases} \tag{3.6}$$

Therefore, $D_h(a(\theta), b(\theta); e^{i\theta h}) = 0$ if and only if

$$\begin{cases} a\cos\theta\bar{\tau} + b\cos\left(\theta\frac{\bar{\tau}}{2}\right) Q(\theta; h) = 1, \\ a\sin\theta\bar{\tau} + b\sin\left(\theta\frac{\bar{\tau}}{2}\right) Q(\theta; h) = 0. \end{cases} \tag{3.7}$$

In addition to the cases $\theta = 0$ and $\theta = 2\pi/h$, already discussed in the general-kernel setting, system (3.7) is singular for $\theta = \frac{2\pi\ell}{\bar\tau}$, $\ell = 1, \ldots, \bar r - 1$. From (3.7), with (3.6), these values of θ lead to the straight lines

$$a + b\tau_\ell(h) = 1, \qquad \ell = 1, \ldots, \bar r - 1, \tag{3.8}$$

with

$$\tau_\ell(h) = e^{-i\pi l} Q\left(\frac{2\pi\ell}{\bar\tau}; h\right) = \begin{cases} 2h \displaystyle\sum_{j=0}^{(\bar r-1)/2} w_j \cos\left(\frac{2\pi\ell j}{\bar r}\right), & \text{if } \bar r \text{ is odd,} \\ h\left(2 \displaystyle\sum_{j=0}^{\bar r/2-1} w_j \cos\left(\frac{2\pi\ell j}{\bar r}\right) + (-1)^\ell\right), & \text{if } \bar r \text{ is even.} \end{cases} \tag{3.9}$$

All the remaining values of θ give points with $a = -1$, which lie on the boundary of the strip $-1 < a < 1$ considered here.

Observe that, for each fixed ℓ, $\tau_\ell(h)$ is the Gregory approximation of

$$\int_0^{\bar\tau} \cos\left(\frac{2\pi\ell\tau}{\bar\tau}\right) d\tau = 0.$$

Hence, for each fixed ℓ, one has $\tau_\ell(h) = O(h^p)$ as $h \to 0$. This estimate is not uniform with respect to ℓ because the constants in the quadrature error bound depend on derivatives of the integrand, which grow with ℓ. In particular, when ℓ ranges over $1, \ldots, \bar r - 1$, the most restrictive negative value among the quantities $\tau_\ell(h)$ may scale only linearly with h, as shown by the examples discussed below. When $p = 2$, the Gregory formula reduces to the trapezoidal rule, which is exact for $\ell = 1, \ldots, \bar r - 1$, due to the periodicity of $\cos\left(\frac{2\pi\ell\tau}{\bar\tau}\right)$ in $[0, \bar\tau]$. As a consequence, $\tau_\ell(h) = 0$ for $\ell = 1, \ldots, \bar r - 1$, and the lines in (3.8) collapse to the limit case $a = 1$. Therefore, the trapezoidal method preserves the continuous stability region of the basic test equation for every admissible stepsize.

For higher order formulas ($p > 2$), one has $|\tau_\ell(h)| < \bar\tau$ for all $\ell = 1, \ldots, \bar r - 1$ so that the numerical region extends the continuous one in the half-plane $b > 0$. Spurious lines arise when $\tau_\ell(h) < 0$, for some ℓ. Figure 5 provides a schematic geometric representation of the strip $(-1, 1) \times \mathbb{R}$, the upper boundary $a + b\bar\tau = 1$, and the additional straight line $a + b\tau_*(h) = 1$, with

$$\tau_*(h) = \tau_{\ell_*}(h), \text{ with } \ell_* : |\tau_{\ell_*}(h)| = \max_\ell\{|\tau_\ell(h)| \text{ with } \tau_\ell(h) < 0\}.$$

Since $\tau_*(h) \to 0$ as $h \to 0$, for any fixed pair $(\bar a, \bar b)$, one can always choose h sufficiently small so that the corresponding point lies inside the stability region (as illustrated in Figure 5). The quantity $\tau_*(h)$ should not be interpreted as an additional physical delay. Rather, it quantifies how far the discrete stability boundary may be shifted from the continuous one.

For the relevant case $\bar b < 0$, it is sufficient to choose h such that

$$|\tau_*(h)| < \frac{\bar a - 1}{\bar b}. \tag{3.10}$$

Figures 6 and 7 illustrate how the bound (3.10) affects the stability of the numerical solution to the basic test equation in representative critical cases.

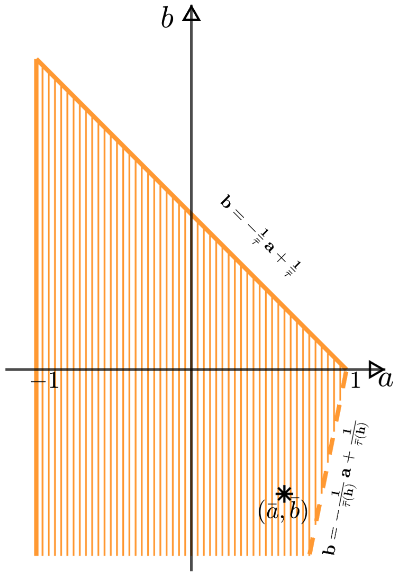

Figure 5. Schematic representation of the strip $(-1, 1) \times \mathbb{R}$, the upper boundary $a + b\bar{\tau} = 1$, and the additional straight line $a + b\tau_*(h) = 1$, with $\tau_*(h) < 0$, arising in the discrete stability analysis of the basic test equation. The point $(\bar{a}, \bar{b})$ illustrates a representative choice of parameters.

We first consider the constant-kernel case $k(\tau) = 1$ with $(a, b) = (0.9, -100)$ and $\bar{\tau} = 10$, discretised by the Gregory method with $p = 3$. For the Gregory method with $p = 3$, one has

$$\tau_\ell(h) = \frac{h}{6}\left(\cos\frac{2\pi\ell}{\bar{r}} - 1\right) \le 0$$

so that

$$|\tau_*(h)| \le \frac{h}{3},$$

with equality if $\bar{r}$ is even. Hence, in the case $\bar{b} < 0$, the sufficient condition (3.10) becomes

$$h < \frac{3(1 - \bar{a})}{|\bar{b}|}.$$

For $(\bar{a}, \bar{b}) = (0.9, -100)$, this gives the bound $h < 0.003$. Figure 6 shows both the numerical solutions and a windowed amplitude indicator, obtained by taking the maximum of $|y(t)|$ over successive delay intervals of length $\bar{\tau}$. In particular, the case $h = 0.5 \cdot 10^{-2}$ is unstable, whereas the case $h = 10^{-3}$ is stable.

We next consider the same constant-kernel setting with $(a, b) = (0.5, -1)$ and $\bar{\tau} = 10$, using the Gregory method with $p = 6$. In this case, when $\bar{b} < 0$, the sufficient condition (3.10) becomes

$$h < \frac{45(1 - \bar{a})}{76|\bar{b}|}.$$

For $(\bar{a}, \bar{b}) = (0.5, -1)$, this gives $h < \frac{45}{152} \approx 0.2961$. Figure 7 displays both the numerical solutions and the corresponding windowed amplitude indicator, again defined as the maximum of $|y(t)|$ over successive delay intervals. In this case, the numerical solution is unstable for $h = 0.5$, while it is stable for $h = 0.25$.

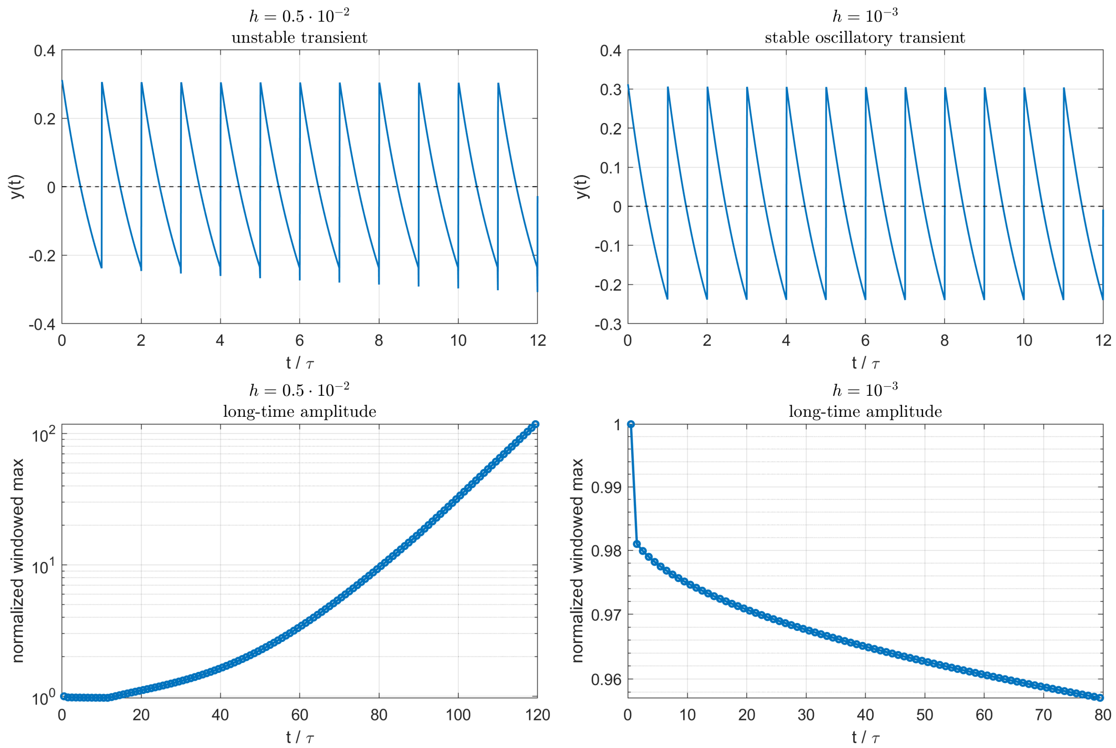

Figure 6. Numerical behaviour for $k(\tau) = 1$, $(a, b) = (0.9, -100)$, and $\bar{\tau} = 10$, using the Gregory method with $p = 3$, with initial function $\varphi(t)$ chosen so as to satisfy the compatibility condition (2.1). Top row: numerical solutions for $h = 0.5 \cdot 10^{-2}$ and $h = 10^{-3}$. Bottom row: corresponding normalised maxima of $|y(t)|$ over successive delay windows. The case $h = 0.5 \cdot 10^{-2}$ is unstable, whereas the case $h = 10^{-3}$ is stable.

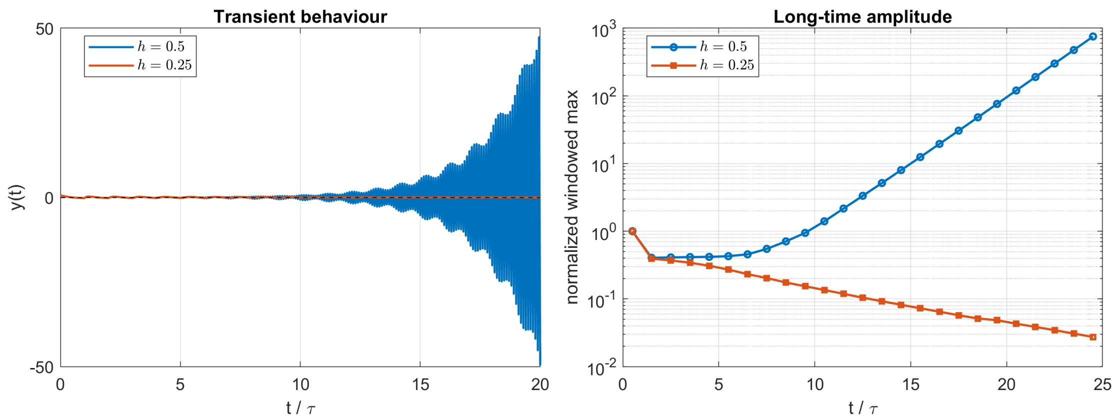

Figure 7. Numerical behaviour for $k(\tau) = 1$, $(a, b) = (0.5, -1)$, and $\bar{\tau} = 10$, using the Gregory method with $p = 6$, with initial function φ chosen so as to satisfy the compatibility condition (2.1). Top row: numerical solutions for $h = 0.5$ and $h = 0.25$. Bottom row: corresponding normalised maxima of $|y(t)|$ over successive delay windows. The case $h = 0.5$ is unstable, whereas the case $h = 0.25$ is stable.

4. General kernels: stability regions and spectral sets

As discussed in Sections 2.2 and 3, apart from the special case of a constant kernel, the analytical study of the boundary systems (2.9) and (3.4) is, in general, difficult. For this reason, in the present section, we focus on sufficient stability conditions and on numerical sets that provide additional information on the location of the continuous and discrete stability regions in the (a, b)-plane for a general continuous kernel k. More precisely, we first introduce sufficient continuous and discrete stability regions, adopting the methodology introduced by Baker and Ford [39] for delay integro-differential equations. We then compare the spectral sets associated with the continuous problem (1.1) and its discrete counterpart (3.1).

As a concrete motivating setting, consider epidemic renewal models with finite infectivity support; see, e.g., [4,5]. If $\bar{\tau} = \sup\{\tau \geq 0 : A(\tau) > 0\}$, then one may consider

$$S'(t) = \lambda - \mu S(t) - S(t)F(t), \qquad F(t) = \int_0^{\bar{\tau}} A(\tau)S(t-\tau)F(t-\tau)\,d\tau.$$

Here, $S(t)$ denotes the susceptible population, $F(t)$ is the force of infection, and $A(\tau)$ is the infectivity function. By integrating the equation for S over an interval of length $\bar{\tau}$, this problem can be rewritten as a system with both a pointwise delay term and a distributed term over the bounded interval $[0, \bar{\tau}]$:

$$\begin{aligned} S(t) &= e^{-\mu\bar{\tau}}S(t-\bar{\tau}) + \int_0^{\bar{\tau}} e^{-\mu\tau}(\lambda - S(t-\tau)F(t-\tau))\,d\tau, \\ F(t) &= \int_0^{\bar{\tau}} A(\tau)S(t-\tau)F(t-\tau)\,d\tau. \end{aligned}$$

After linearisation around an equilibrium, one is thus led to linear systems with the same structural features as the test equations studied here. From this viewpoint, the kernels used in the numerical examples below may be interpreted as finite-memory infectivity profiles, while the present scalar analysis provides preliminary information on the stability properties that a numerical discretisation should preserve in more complex epidemic models.
We begin with the following sufficient continuous stability condition.

Theorem 4.1. *The zero solution of (1.1) is asymptotically stable if*

$$(a, b) \in \mathcal{W} := \left\{(a, b) \in \mathbb{R}^2 : \ |a| + |b| \int_0^{\bar{\tau}} k(\tau)\,d\tau < 1\right\}. \tag{4.1}$$

Proof. We write the stability function in (2.4) as $D(a, b; \omega) = d_1(\omega) - d_2(\omega)$, with $d_1(\omega) = 1 - ae^{-\omega\bar{\tau}}$ and $d_2(\omega) = b\int_0^{\bar{\tau}} e^{-\omega\tau}k(\tau)d\tau$. By applying Rouché's theorem, it follows that $D(a, b; \omega)$ admits no zeros in the half-plane $Re(\omega) \geq 0$. Consequently, all characteristic roots satisfy $Re(\omega) < 0$, ensuring asymptotic stability of (1.1). □

Analogous reasoning to that employed in Theorem 4.1 yields the corresponding stability region for the discrete formulation (3.1), namely

$$\mathcal{W}_h = \left\{(a, b) \in \mathbb{R}^2 : \ |a| + |b|\, h \sum_{j=0}^{\bar{r}} w_j k(t_j) < 1\right\}. \tag{4.2}$$

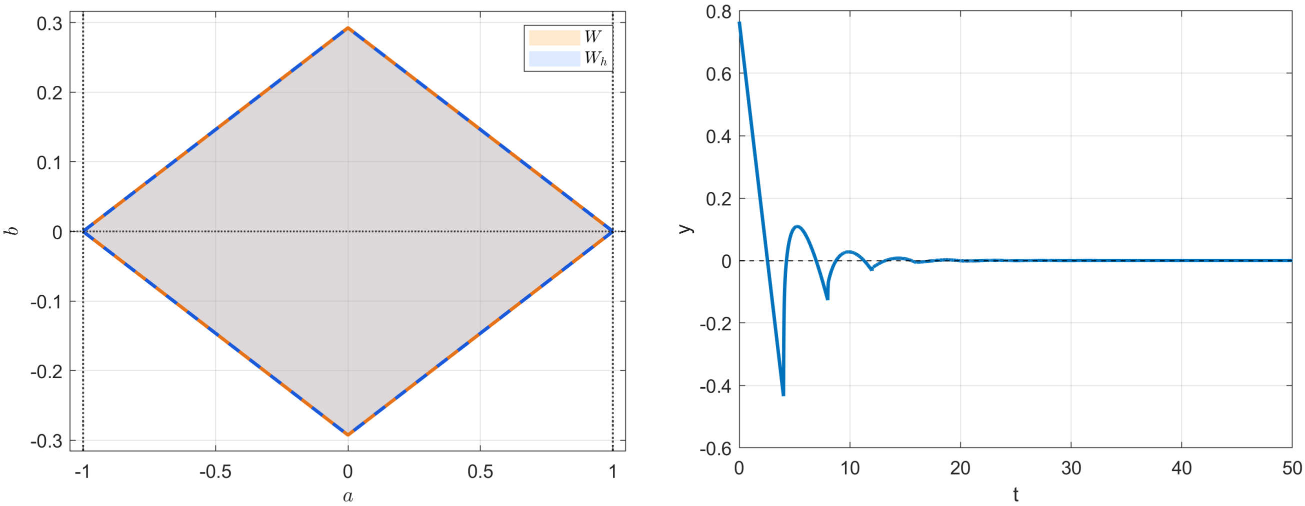

Figure 8. Left: continuous and discrete sufficient stability regions in the (a, b)-plane. Right: stable solution obtained with method (3.1), with $p = 5$ and $h = 0.5 \cdot 10^{-2}$. Here, $k(\tau) = (\tau + 0.1)^{-1/2}$, $\bar{\tau} = 4$, $a = 0.3$ and $b = -10$, with initial function φ chosen so as to satisfy the compatibility condition (2.1).

Let p denote the order of accuracy of the numerical method. From (4.1) and (4.2), it follows that if k is a polynomial of degree at most $p - 1$, then $\mathcal{W}_h = \mathcal{W}$, since the Gregory quadrature formula of order p is exact on polynomials up to degree $p - 1$. Conversely, when k is not a polynomial of the corresponding degree, then $\mathcal{W}_h$ converges to $\mathcal{W}$ as $h \to 0$, with an $O(h^p)$ error in the slope of the boundary lines.

Figure 8 (left panel) illustrates the theoretical sufficient stability regions $\mathcal{W}$, for $k = 1/(\tau + 0.1)^{1/2}$, together with its discrete counterpart $\mathcal{W}_h$ obtained with $h = 0.5 \cdot 10^{-2}$ and the order $p = 5$ quadrature scheme. For $b > 0$, and in view of (2.10) and (3.5), the bounds defined by $\mathcal{W}$ and $\mathcal{W}_h$ coincide with the upper stability thresholds provided by the continuous and discrete boundary relations. In contrast, when $b < 0$, these bounds provide only a sufficient condition, which tends to be overly restrictive, as clearly evidenced by the numerical result shown in Figure 8 (right panel) where the pair $(a, b) = (0.3, -10)$ is chosen outside the sufficient stability region.

To gain insight into specific cases, we extend the approach presented by Luzyanina et al. [26] for delay integral equations.

We write $D_h(a, b; e^{-\omega h}) = 1 - \Psi_h(\omega)$ with

$$\Psi_h(\omega) = a e^{-\omega\bar{\tau}} + bh \sum_{j=0}^{\bar{r}} w_j k(t_j) e^{-\omega h j}.$$

Then

$$\Sigma_h(\mathbb{C}^+) = \bigcup_{\omega \in \mathbb{C}^+} \Psi_h(\omega)$$

is a bounded set of $\mathbb{C}$. The boundary of $\Sigma_h(\mathbb{C}^+)$ is given by the curve

$$\bigcup_{\theta \in [0, 2\pi/h]} \Psi_h(i\theta).$$

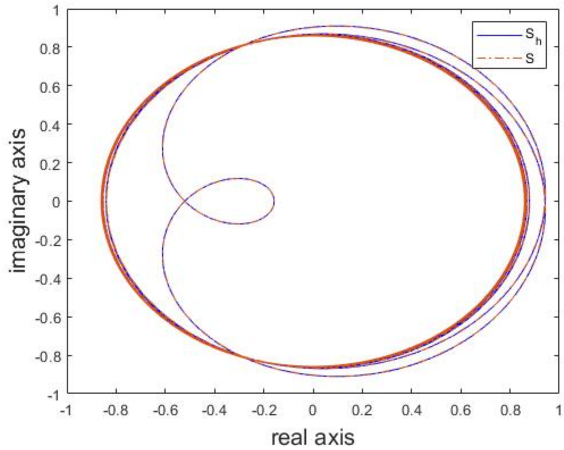

Figure 9. Boundaries of the sets Σ_h (solid line) and Σ (dashed-dotted line), $p = 2$, $\bar{\tau} = 15$, $h = 0.1$, $a = 0.86$, $b = -0.01$ and $k(\tau) = \tau e^{-0.01\tau}$.

The plot of the boundary of $\Sigma_h(\mathbb{C}^+)$ is shown in Figure 9 (solid line); for the trapezoidal $p = 2$ method, $\bar{\tau} = 15$, $h = 0.1$, $a = 0.86$, $b = -0.01$ and $k(\tau) = \tau e^{-0.01\tau}$. The dashed-dotted line in the same figure represents the boundary of the corresponding set $\Sigma(\mathbb{C}^+) = \left\{ae^{-\omega\bar{\tau}} + b\int_0^{\bar{\tau}} e^{-\omega\tau}k(\tau)d\tau, \ : \ \omega \in \mathbb{C}^+\right\}$, related to (2.4). This representation enables a graphical analysis of whether the rightmost intersection of $\Sigma_h(\mathbb{C}^+)$ with the real axis lies to the left of 1, which indicates stability of the Gregory method, and of how accurately it approximates the corresponding intersection point of $\Sigma(\mathbb{C}^+)$.

To illustrate that stable configurations may also occur for $a > 1$, we consider the normalized kernel

$$k_\sigma(\tau) = C_\sigma \exp\left(-\frac{(\bar{\tau}-\tau)^2}{\sigma^2}\right), \qquad C_\sigma^{-1} = \int_0^{\bar{\tau}} \exp\left(-\frac{(\bar{\tau}-s)^2}{\sigma^2}\right) ds, \tag{4.3}$$

with $\bar{\tau} = 1$ and $\sigma = 5 \cdot 10^{-3}$. For the parameter choice $(a, b) = (1.05, -0.2)$, numerical inspection of the continuous characteristic equation reveals no roots in the half-plane $Re(\omega) \geq 0$, although $a > 1$. This indicates that the negative distributed-delay contribution compensates the destabilizing effect of the pointwise delay term. The same behaviour is reproduced by the trapezoidal discretisation: for instance, with $h = 0.05, 0.02, 0.01$, all computed discrete characteristic roots lie inside the unit disk. Figure 10 illustrates the corresponding stable numerical behaviour.

5. Conclusion

In this paper, we have investigated the stability properties of quadrature-based approximations for a class of linear Volterra integral equations involving both a discrete delay and a bounded distributed delay. The analysis has been carried out in parallel for the continuous problem and for its discrete counterpart, by combining the Laplace-transform and spectral arguments with a boundary-locus approach.

The equation studied here should be viewed as a scalar prototype for more general linearised systems in which a pointwise delay term is coupled with a distributed memory term over a bounded

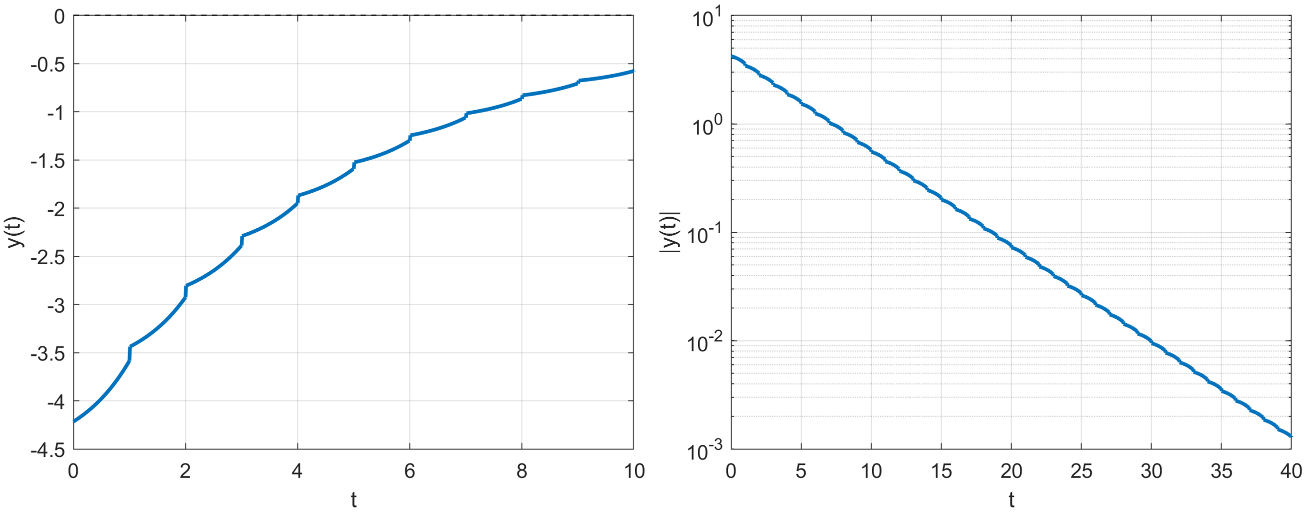

Figure 10. Numerical example with $a > 1$ and $b < 0$ for a non-constant distributed-delay kernel (4.3). Here $\bar{\tau} = 1$, $a = 1.05$, $b = -0.2$. The initial function is chosen to satisfy the compatibility condition (2.1). Left: numerical solution obtained by the trapezoidal discretisation. Right: semilogarithmic plot of $|y(t)|$ over a longer time interval.

interval. This structure arises naturally in several applications, including epidemic renewal models with finite memory.

For the basic test equation with a constant kernel, the analysis yields an explicit description of the discrete stability region and practical stepsize restrictions ensuring stability preservation. For general kernels, the boundary systems are no longer explicitly solvable; nevertheless, the comparison between the continuous and discrete boundary loci shows that the reconstruction of the stability geometry is governed by the quadrature approximation errors. In this setting, the sufficient stability regions and the spectral-set analysis developed in Section 4 provide additional information on the location of the continuous and discrete stability domains.

Several directions remain open. It would be useful to derive a closed-form expression for the stepsize bound discussed in Section 3. It would also be natural to consider other classes of test equations with non-constant kernels, such as kernels of convolution type or completely monotone kernels, which often arise in numerical stability theory. Finally, extending the present framework to systems of equations, possibly coupled with other types of functional equations, would make it possible to analyse the linear stability properties of recently proposed epidemic models, such as those introduced by Buonomo et al. [40], particularly when the infectivity function has compact support.

These perspectives are especially relevant in mathematical biology, where linear integral equations with finite memory arise naturally in the stability analysis of renewal, epidemic, and population models. In such contexts, preserving the stability properties in the numerical solution is essential for obtaining reliable long-time predictions. This line of research is also related to recent pseudospectral techniques developed for renewal equations and for epidemic models with structured or renewal-type dynamics; see, e.g., [41–43].

Use of AI tools declaration

The authors declare they have not used Artificial Intelligence (AI) tools in the creation of this article.

Acknowledgments

The authors are grateful to the anonymous Referees for their careful reading of the manuscript and for their valuable comments and suggestions, which contributed to improving both the presentation and the content of the paper. E.M. is partially supported by INdAM, through GNCS research projects and by PRIN 2022XZSAFN "Anomalous Phenomena on Regular and Irregular Domains: Approximating Complexity for the Applied Sciences".

Conflict of interest

The authors declare there is no conflict of interest.

References

1. H. Brunner, *Volterra integral equations: an introduction to theory and applications*, Cambridge Monographs on Applied and Computational Mathematics, Cambridge, 2017. https://doi.org/10.1017/9781316162491
2. G. Gripenberg, S. O. Londen, O. J. Staffans, *Volterra Integral and Functional Equations*, Cambridge University Press, Cambridge, 1990. https://doi.org/10.1017/CBO9780511662805
3. R. Bellman, K. L. Cooke, *Differential-Difference Equations*, Academic Press, New York & London, 1963.
4. N. Hritonenko, C. Satsky, Y. Yatsenko, Integral model of COVID-19 spread and mitigation in UK: identification of transmission rate, *Math. Model. Anal.*, **27** (2022), 573–589. https://doi.org/10.3846/mma.2022.15708
5. M. T. Meehan, D. G. Cocks, J. Müller, E. S. McBryde, Global stability properties of a class of renewal epidemic models, *J. Math. Biol.*, **78** (2019), 1713–1725. https://doi.org/10.1007/s00285-018-01324-1
6. H. W. Hethcote, H. W. Stech, P. v. d. Driessche, Periodicity and stability in epidemic models: A survey, in *Differential Equations and Applications in Ecology, Epidemics, and Population Problems*, Academic Press, 1981, 65–82. https://doi.org/10.1016/b978-0-12-148360-9.50011-1
7. E. Beretta, D. Breda, Discrete or distributed delay effects on stability of population growth, *Math. Biosci. Eng.*, **13** (2016), 19–41. https://doi.org/10.3934/mbe.2016.13.19
8. M. Courtemanche, J. P. Keener, L. Glass, A delay equation representation of pulse circulation on a ring in excitable media, *SIAM J. Appl. Math.*, **56** (1996), 119–142. https://doi.org/10.1137/S0036139993259337
9. I. Balogoun, J. Auriol, I. Boussaada, G. Mazanti, A novel necessary and sufficient condition for the stability of 2×2 first-order linear hyperbolic systems, *Syst. Control Lett.*, **199** (2025), 106066. https://doi.org/10.1016/j.sysconle.2025.106066

10. J. Auriol, Stabilization of integral delay equations by solving Fredholm equations, *IEEE Control Syst. Lett.*, **8** (2024), 676–681. https://doi.org/10.1109/LCSYS.2024.3402130

11. D. Melchor-Aguilar, Exponential stability of some linear continuous time difference systems, *Syst. Control Lett.*, **61** (2012), 62–68. https://doi.org/10.1016/j.sysconle.2011.09.013

12. D. Melchor-Aguilar, On the equivalence of L2-exponential and exponential stability of linear functional difference systems, *J. Math. Anal. Appl.*, **553** (2026), 129958. https://doi.org/10.1016/j.jmaa.2025.129958

13. G. Ochoa-Ortega, M. A. Gomez, Critical parameters for a class of integral difference equations, *Int. J. Robust Nonlinear Control*, **32** (2022), 3141–3151. https://doi.org/10.1002/rnc.5816

14. H. Brunner, P. van der Houwen, *The numerical solution of Volterra equations*, CWI monographs, North-Holland, 1986.

15. B. Buonomo, E. Messina, C. Panico, A. Vecchio, A stable numerical method for integral epidemic models with behavioral changes in contact patterns, *Electron. Trans. Numer. Anal.*, **61** (2024), 137–156. https://doi.org/10.1553/etna_vol61s137

16. E. Messina, M. Pezzella, A. Vecchio, Nonlocal finite difference discretization of a class of renewal equation models for epidemics, *Math. Biosci. Eng.*, **20** (2023), 11656–11675. https://doi.org/10.3934/mbe.2023518

17. J. Ripoll, J. Font, Numerical approach to an age-structured Lotka-Volterra model, *Math. Biosci. Eng.*, **20** (2023), 15603–15622. https://doi.org/10.3934/mbe.2023696

18. A. Wendler, L. Plötzke, H. Tritzschak, M. J. Kühn, A nonstandard numerical scheme for a novel SECIR integro-differential equation-based model allowing nonexponentially distributed stay times, *Appl. Math. Comput.*, **509** (2026), 129636. https://doi.org/10.1016/j.amc.2025.129636

19. A. Abdi, J. Berrut, S. A. Hosseini, The linear barycentric rational method for a class of delay Volterra integro-differential equations, *J. Sci. Comput.*, **75** (2018), 1757–1775. https://doi.org/10.1007/s10915-017-0608-3

20. A. Hosseinian, P. Assari, M. Dehghan, The numerical solution of nonlinear delay Volterra integral equations using the thin plate spline collocation method with error analysis, *Comput. Appl. Math.*, **42** (2023), 1–24. https://doi.org/10.1007/s40314-023-02219-8

21. D. Conte, E. Farsimadan, L. Moradi, F. Palmieri, B. Paternoster, Numerical solution of delay Volterra functional integral equations with variable bounds, *Appl. Numer. Math.*, **200** (2024), 148–161. https://doi.org/10.1016/j.apnum.2023.05.002

22. P. Darania, F. Sotoudehmaram, Numerical analysis of a high order method for nonlinear delay integral equations, *J. Comput. Appl. Math.*, **374** (2020), 112738. https://doi.org/10.1016/j.cam.2020.112738

23. H. Brunner, *Collocation Methods for Volterra Integral and Related Functional Differential Equations*, Cambridge Monographs on Applied and Computational Mathematics, Cambridge, 2004. https://doi.org/10.1017/CBO9780511543234

24. C. T. H. Baker, N. J. Ford, Some applications of the boundary-locus method and the method of D-partitions, *IMA J. Numer. Anal.*, **11** (1991), 143–158. https://doi.org/10.1093/imanum/11.2.143

25. C. T. H. Baker, M. S. Derakhshan, Convergence and stability of quadrature methods applied to Volterra equations with delay, *IMA J. Numer. Anal.*, **13** (1993), 67–91. https://doi.org/10.1093/imanum/13.1.67
26. T. Luzyanina, D. Roose, K. Engelborghs, Numerical stability analysis of steady state solutions of integral equations with distributed delays, *Appl. Numer. Math.*, **50** (2004), 75–92. https://doi.org/10.1016/j.apnum.2003.12.001
27. E. Messina, E. Russo, A. Vecchio, A convolution test equation for double delay integral equations, *J. Comput. Appl. Math.*, **228** (2009), 589–599. https://doi.org/10.1016/j.cam.2008.03.047
28. C. Lubich, Runge–Kutta theory for Volterra and Abel integral equations of the second kind, *Math. Comput.*, **41** (1983), 87–102. https://doi.org/10.1090/S0025-5718-1983-0701626-6
29. C. Lubich, On the stability of linear multistep methods for Volterra convolution equations, *IMA J. Numer. Anal.*, **3** (1983), 439–465. https://doi.org/10.1093/imanum/3.4.439
30. L. F. Shampine, S. Thompson, Numerical solution of delay differential equations, in *Delay Differential Equations*, Springer, Boston, MA, 2009. https://doi.org/10.1007/978-0-387-85595-0_9
31. D. Breda, S. Maset, R. Vermiglio, *Stability of Linear Delay Differential Equations: A Numerical Approach with MATLAB*, Springer, New York, 2015. https://doi.org/10.1007/978-1-4939-2107-2
32. M. M. Moghaddam, H. D. Mazraeh, K. Parand, A double deep q network-powered approach to discovering symbolic solutions for nonlinear integral equations, *Eng. Appl. Artif. Intell.*, **169** (2026), 114113. https://doi.org/10.1016/j.engappai.2026.114113
33. M. M. Moghaddam, H. D. Mazraeh, K. Parand, Symbolic solution of fractional Volterra population models via physics-informed neural networks and distributed particle swarm optimization, *Appl. Soft Comput.*, **189** (2026), 114512. https://doi.org/10.1016/j.asoc.2025.114512
34. H. D. Mazraeh, A. N. Firoozsalari, A. A. Aghaei, K. Parand, A novel neural network architecture for solving fractional differential equations, *Comput. Methods Differ. Equat.*, Advance online publication. https://doi.org/10.22034/cmde.2025.63059.2803
35. P. M. Anselone, D. Greenspan, On a class of linear difference-integral equations, *Arch. Ration. Mech. An.*, **13** (1963), 59–80.
36. J. Chen, K. H. Lundberg, D. E. Davison, D. S. Bernstein, The final value theorem revisited - infinite limits and irrational functions, *IEEE Control Syst.*, **27** (2007), 97–99. https://doi.org/10.1109/MCS.2007.365008
37. O. Diekmann, M. Gyllenberg, Equations with infinite delay: Blending the abstract and the concrete, *J. Differ. Equat.*, **252** (2012), 819–851. https://doi.org/10.1016/j.jde.2011.09.038
38. S. N. Elaydi, *An Introduction to Difference Equations*, 3rd edition, Springer, New York, 2005. https://doi.org/10.1007/0-387-27602-5
39. C. T. H. Baker, N. J. Ford, Stability properties of a scheme for the approximate solution of a delay-integro-differential equation, *Appl. Numer. Math.*, **9** (1992), 357–370. https://doi.org/10.1016/0168-9274(92)90027-B
40. B. Buonomo, E. Messina, C. Panico, A. Vecchio, An integral renewal equation approach to behavioural epidemic models with information index, *J. Math. Biol.*, **90** (2025), 1–26. https://doi.org/10.1007/s00285-024-02172-y

41. D. Breda, O. Diekmann, D. Liessi, F. Scarabel, Numerical bifurcation analysis of a class of nonlinear renewal equations, *Electron. J. Qual. Theo.*, **65** (2016), 1–24. https://doi.org/10.14232/ejqtde.2016.1.65

42. D. Breda, D. Liessi, A practical approach to computing Lyapunov exponents of renewal and delay equations, *Math. Biosci. Eng.*, **21** (2024), 1249–1269. https://doi.org/10.3934/mbe.2024053

43. F. Scarabel, O. Diekmann, R. Vermiglio, Numerical bifurcation analysis of renewal equations via pseudospectral approximation, *J. Comput. Appl. Math.*, **397** (2021), 113611. https://doi.org/10.1016/j.cam.2021.113611